



CHORUS

This is the accepted manuscript made available via CHORUS. The article has been published as:

Tip-induced local strain on MoS₂/graphite detected by inelastic electron tunneling spectroscopy

Wonhee Ko, Saban M. Hus, Xufan Li, Tom Berlijn, Giang D. Nguyen, Kai Xiao, and An-Ping Li

Phys. Rev. B **97**, 125401 — Published 2 March 2018

DOI: [10.1103/PhysRevB.97.125401](https://doi.org/10.1103/PhysRevB.97.125401)

Tip-induced local strain on MoS₂/graphite detected by inelastic electron tunneling spectroscopy

Wonhee Ko¹, Saban M. Hus¹, Xufan Li¹, Tom Berlijn^{1,2}, Giang D. Nguyen¹, Kai Xiao¹, An-Ping Li¹

¹ *Center for Nanophase Materials Sciences, Oak Ridge National Laboratory, Oak Ridge, TN 37831, USA*

² *Computational Sciences & Engineering Division, Oak Ridge National Laboratory, Oak Ridge, TN 37831, USA*

Abstract

We report the detection of tip-induced local strain applied to the monolayer MoS₂ grown on a graphite substrate by scanning tunneling microscope (STM). Monolayer MoS₂ behaves as both mechanical and tunneling barriers that prevent the tip from contacting the graphite while maintaining the tunneling current. Inelastic tunneling electron spectroscopy (IETS) is utilized to probe the phonon modes in graphite. As the tip pushes the sample, IETS reveals a continuous phonon-softening in graphite, corroborated by a downward shift of the phonon energy as calculated by density functional theory. Our results demonstrate a novel way to apply local mechanical strain and simultaneously detect the induced change in phonon modes by unitizing IETS with two-dimensional materials as a tunneling barrier.

PACS number(s):

1. Introduction

Two-dimensional (2D) materials such as graphene and transition metal dichalcogenides are promising candidates for next-generation electronics due to not only their superior electronic properties but also their high mechanical strength. Extreme toughness against mechanical stress makes them suitable for novel applications as flexible display and wearable devices ¹. Mechanical stress can alter their electronic properties such as changing the electronic band gap and introducing pseudo-magnetic field ²⁻⁴, and thus the strain engineering is an active research field for 2D materials ⁵. Because the materials are so thin with only a few atoms thick, scanning probe microscopy (SPM) has been utilized to locally strain the materials and measure their mechanical responses. Especially, atomic force microscopy (AFM) has been widely used to observe the deformation of suspended 2D materials in response to the tip-induced local force ⁶⁻⁸. However, AFM usually measures static response like the stress-strain curve, and studies on dynamic response like strain-induced changes in vibrational and phononic properties are rare. Also, AFM is not optimized for measuring the materials' electronic properties, so it is still challenging to measure both local strain and its effect on electronic properties at the same time. To overcome the disadvantages of AFM, there were attempts to combine Raman spectroscopy with AFM and observe local phonon properties, and a recent study showed that the strain induced by AFM tip was detectable by tip-enhanced Raman spectroscopy ⁹.

Inelastic tunneling electron spectroscopy (IETS) is a method capable of directly observing phonons by exciting them with tunneling electrons ¹⁰⁻¹⁶. Especially, IETS performed by scanning tunneling microscopy (STM) can measure the phonons at the nanoscale, which was successfully demonstrated in graphene ^{11,12,14}. By adjusting tip-sample separation in sub-nanometer scale with STM, the tip-induced change in the phonon energy of

molecules was detected, too¹⁷. However, IETS signals are usually an order of magnitude weaker than the one from ordinary scanning tunneling spectroscopy (STS), and so the sophisticated vibration isolation system with operating temperature less than 10 K is usually required to maintain stable vacuum tunneling barrier¹⁶. Replacing the vacuum barrier with a few layers of hexagonal boron nitride (hBN) is considered as a method to create more stable tunneling barrier for IETS, and several devices in this scheme have successfully measured phonons in graphene and hBN^{10, 15, 18}. However, it is hard to apply strain to such devices because the entire device area should be uniformly strained, which is usually larger than a micrometer, and the local information is disguised under the macroscopic average properties. Conventional straining methods such as cantilever beams or diamond anvil cells achieved a maximum strain of about 1% or less¹⁹⁻²².

Here we utilize monolayer MoS₂ grown on graphite as a tunneling barrier to perform IETS with STM. The recent development of chemical vapor deposition technique enabled uniform large-scale epitaxial growth of monolayer transition metal dichalcogenides, which is a strong advantage of MoS₂ compared to hBN^{23, 24}. As a semiconductor with a bandgap of 2.1 eV²⁵⁻²⁹, monolayer MoS₂ behaves as a tunneling barrier for electron transport to the graphite substrate at low bias. Moreover, its high mechanical strength enables application of mechanical strain to the graphite underneath with the STM tip^{6, 8}. IETS reveals a downward shift of the phonon energy as the tip pushes the sample, and the shift increases with the tip-induced strain. Compared with the calculated phonon density of the states (DOS), the IETS results allow us to correlate the local strain with the phonon energies of graphite.

2. Experiment and Methods

MoS₂ was grown by chemical vapor deposition on highly oriented pyrolytic graphite

(HOPG) substrate³⁰. MoS₂ forms a few micrometer size triangular patches with mostly monolayer and occasionally small regions of bi- or multilayer. For the STM measurement, Omicron variable temperature STM (VT STM) and a cryogenic 4 probe STM (4P STM) were utilized. VT STM was operated at room temperature to image the sample down to the atomic scale, while 4P STM was used to measure spectroscopy since it is more thermally stable at low temperature (82 K)³¹⁻³³. Also, scanning electron microscope (SEM) attached to the 4 probe STM allows finding the micrometer-size patches of monolayer MoS₂. Both systems are operated at ultrahigh-vacuum ($\sim 10^{-10}$ torr). STM tips were etched from the tungsten wire and checked by SEM to have the radius of curvature less than 100 nm. Bias voltage V_B was applied to the sample for all STM measurements. For spectroscopy, conventional lock-in amplifier technique was used for measuring differential conductivity dI/dV , where modulation voltage was set to 3~10 mV and modulation frequency to 731 Hz. For IETS, the numerical derivative of dI/dV spectra was taken to extract d^2I/dV^2 . The phonon DOS of graphite was calculated with the DFT based frozen phonon method as implemented in phonopy³⁴ using $4 \times 4 \times 2$ sized supercells. The unstrained crystal structure was taken from Ref.³⁵ for the calculation. For the strained cases, the strain of the in-plane lattice constants was compensated by a reduction of the out-of-plane lattice constants such that the volume of the unit cell remained constant. The DFT calculations were performed within the generalized gradient approximation (GGA) using the Perdew–Burke–Ernzerhof exchange correlation scheme³⁶ and projector augmented wave potentials³⁷ as implemented in VASP^{38,39}. We used a 500 eV kinetic energy cutoff and a $5 \times 5 \times 2$ k-point grid for the supercell calculations.

3. Results and Discussion

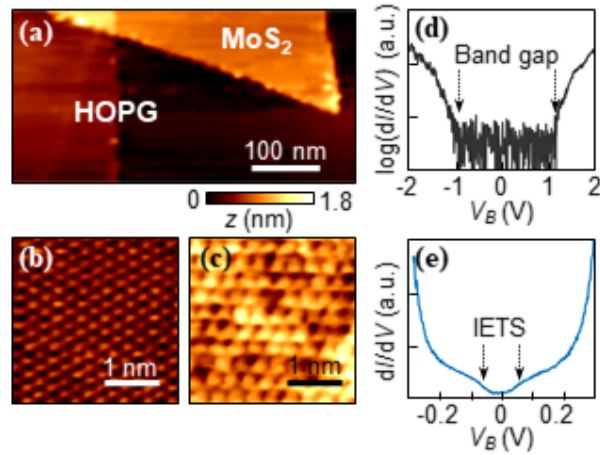


Fig. 1. (a) A large-scale topography image of MoS₂ flake on HOPG ($V_B = 2.0$ V, $I = 50$ pA). (b) Atomic resolution topography images taken on HOPG ($V_B = 0.5$ V, $I = 20$ pA), and (c) monolayer MoS₂ ($V_B = 0.7$ V, $I = 300$ pA). (d) A dI/dV spectrum taken on monolayer MoS₂ with high bias set point ($V_B = 2.0$ V, $I = 20$ pA). (e) dI/dV spectroscopy on monolayer MoS₂ with low bias set point ($V_B = 0.3$ V, $I = 50$ pA).

Atomic structure of MoS₂ flakes was observed by taking topography images with STM at room temperature. Figure 1(a) shows the large-scale topography image of a MoS₂ flake on HOPG surface. The MoS₂ flake on the upper right corner shows typical triangular shape with the height of about 7 Å, while the HOPG step on the left shows only the height of about 3 Å²⁵. Zoomed in topography images on both HOPG and monolayer MoS₂ regions show triangular lattices with lattice constants of 2.4 Å and 3.1 Å, respectively [Figs. 1(b) and (c)], which matches the reported values^{35, 40}. Also, the MoS₂ surface displayed larger corrugation compared to the HOPG, probably due to the defects created during the growth process⁴¹. Subsequently, electronic structure of MoS₂ was probed by dI/dV spectroscopy, performed at the low temperature of 82 K to reduce the thermal broadening. Figure 1(d) shows the typical dI/dV spectrum taken over the monolayer MoS₂, which shows the bandgap

of about 2.1 eV^{25-27, 29}. Here the bias voltage V_B is set to 2.0 V to assure that the tip and the sample are not in contact and no electrons are tunneling into the HOPG. At this high bias set point, dI/dV is negligible inside the band gap. However, when we lower the bias set point to 0.3 V, we observed the finite dI/dV inside the bandgap again [Fig. 1(e)]. Because the bias is lower than the conduction band edge of MoS₂, this finite dI/dV should come from the electrons tunneling into the graphite across the layer of MoS₂. Moreover, there is a gap-like feature around the Fermi energy which is symmetric with a size about 120 meV. This gap-like feature can be identified as an IETS signal induced by the phonon excitations in graphite because of its symmetric shape at the Fermi energy and the size consistent with the energy range of the phonons^{13, 42}.

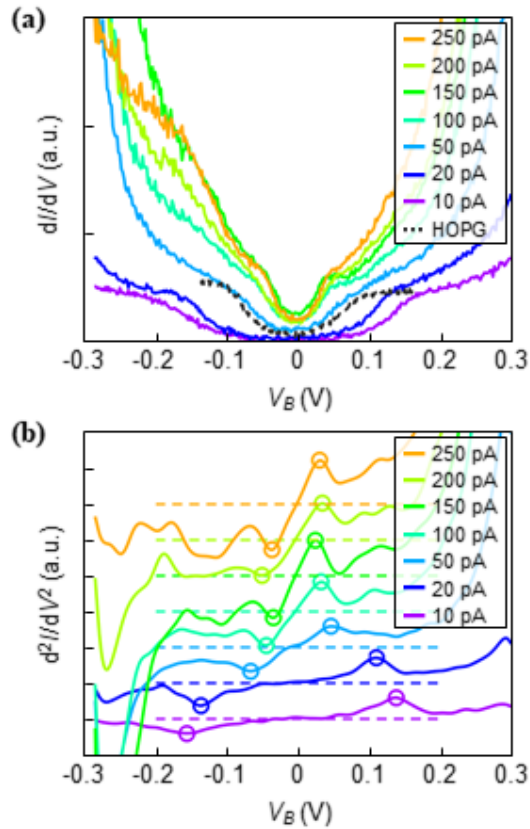


Fig. 2. (a) dI/dV spectra taken at the same location on monolayer MoS_2 with different set point currents as indicated in the labels (set point bias $V_B = 0.3$ V for all spectra). A spectrum taken on bare HOPG surface is plotted together in dashed gray line for comparison (set point $V_B = 0.3$ V, $I = 10$ pA). (b) d^2I/dV^2 spectra derived from numerical derivative of dI/dV spectra in (a). Each spectrum is shifted vertically for clarity, and the horizontal line crossing zero is drawn with dotted lines.

Interestingly, the IETS signal exhibits a strong dependence on the set point current. Figures 2(a) and (b) show the dI/dV and d^2I/dV^2 spectra, respectively, taken at the same location on monolayer MoS_2 with different set point currents. All dI/dV spectra show IETS signal with gap-like features at the Fermi energy, and the gap size decreases as the set point current increases. In d^2I/dV^2 spectra, IETS signal is more clearly shown as symmetric peak-valley pairs across the Fermi level and they shift toward the lower energy as the set point current increases. Peak energy starts from about 150 meV at the lowest set point current of 10 pA, and shifts all the way down to 40 meV at the highest set point current of 250 pA. As the MoS_2 phonons have energies only up to 60 meV⁴³⁻⁴⁵, the IETS peaks in d^2I/dV^2 cannot come from the MoS_2 phonons. On the other hand, phonons in graphite have energy from zero to 200 meV^{13, 15, 42}, and thus we believe that most of the IETS signal here originates from the phonon excitation in graphite. This assignment is supported by a comparison with the dI/dV spectra taken on the bare graphite surface [Fig. 2(a)] which shows the gap structure from the IETS with the similar size. The observation is also consistent with the fact that the electron tunneling occurs between the tip and graphite, instead of MoS_2 .

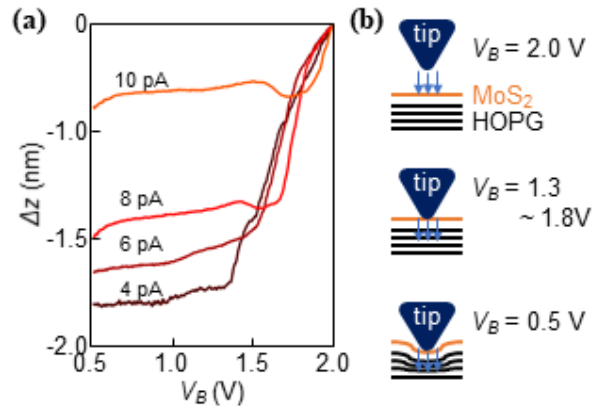


Fig. 3. (a) Changes of the tip height z as a function of the bias voltage for different set point currents (Δz is set to zero at $V_B = 2.0$ V for each curve). (b) Schematics showing the configurations of the tip and the sample for different bias voltages.

To investigate the origin of the shift in the IETS signal, we measured tip height z spectroscopy and examined z dependence on the bias and current. Because the phonon frequency is intimately linked to the mechanical behaviors of the materials, it is important to evaluate the geometry changes of the sample surface with tip height at different set points. Figure 3(a) shows relative tip height Δz while the bias is changing from 2.0 V to 0.5 V for different set point currents. The tip is shown to move toward the sample rapidly to maintain a constant current as the bias decreases, and then move significantly slower after a cusp at 1.3 ~ 1.8 V. This indicates that the tip movement is impeded due to the contact of the tip with the MoS₂ layer at lower bias. Moreover, in contrast to the general trend of decreasing Δz , there is an upturn in Δz slightly below the bias cusp for set point currents larger than 6 pA. It is speculated that the MoS₂ layer starts to move towards the tip as the two come in contact,

which gives rise to a small tip retraction in order to maintain a constant current, especially at high set point currents. Decreasing the bias further from this point requires the tip height becomes lower than the surface of the MoS₂ layer, which will push the sample and strain the sample underneath the tip. The cusp point appears sooner (at lower $|\Delta z|$) when the set point current is increased since the tip is closer to the sample for larger set point current. Figure 3(b) illustrates the tip-sample configurations for the different bias conditions. Note, during these measurements, there was no noticeable damage to the MoS₂ layer as confirmed by STM images, and dI/dV spectra were reproducible before and after applying the strain.

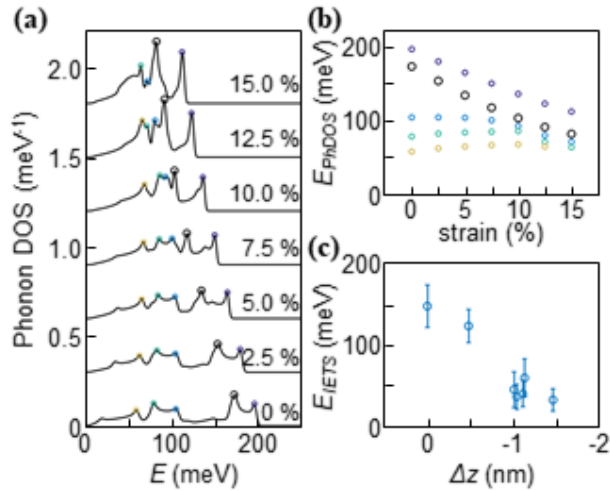


Fig. 4. (a) Calculated phonon DOS of graphite for in-plane strains in the range of 0 % to 15 % (with out-of-plane strains reduced to keep the unit cell volume constant). Peaks in phonon DOS are marked with circles, and the most prominent one in each curve is emphasized with a larger black circle. Each curve is shifted vertically for clarity. (b) Energies of the peaks in phonon DOS as a function of strain extracted from (a), marked with the same color. (c) Measured energy changes of the IETS peaks in Fig 2(b) as a function of the tip height (Δz is set to zero for the set point $V_B = 0.3$ V and $I = 10$ pA). Error bar is FWHMs of the Gaussian

fitting to the IETS peaks.

The effect of the strain on the phonon DOS of graphite was calculated by DFT and compared with the IETS results. To model the experiment condition, we considered the graphite lattice that is stretched in-plane but compressed out-of-plane to keep the unit cell volume constant. We focused on the relationship between in-plane strains and phonon DOS because out-of-plane strains had a negligible effect due to the much weaker bonding in that direction. When the in-plane tensile strain is applied to the graphite, it is expected that phonon energies will decrease because of the weakening of the bonds between the carbon atoms¹⁹⁻²². Graphs of calculated phonon DOS, as shown in Fig. 4(a), shift clearly towards lower energies when increasing the strain level. Prominent peaks in the phonon DOS are plotted as a function of strain in Fig. 4(b), and the peak energies obtained from IETS spectra shown in Fig. 2(b) are plotted as a function of tip height in Fig. 4(c). The peak energy of calculated phonon DOS decreases almost linearly as the strain increases, which is consistent with the changes of measured IETS peaks as a function of tip height. The IETS peak shifts about 100 meV when Δz changes from 0 nm to -1.4 nm, which corresponds to a strain about 10 % for the most prominent phonon peak to shift the same amount. A rough estimation of the strain is also given by $\varepsilon \approx (\Delta z/w)^2$, where ε is the in-plane strain, Δz is indentation depth, and w is the width of the contact^{4,7}. Assuming that the tip radius of curvature $R_{tip} = 5\sim 15$ nm, $\varepsilon \approx 3\sim 5$ % for $\Delta z = 1.4$ nm. Both estimations give the same order of the magnitude of mechanic strain, confirming strain as the cause of the peak shift in IETS. Because of unknown factors such as tip shape, absolute tip height, and geometry of the sample deformation, quantitative analysis is not feasible on the tip-induced strain. In addition, large thermal broadening at the experimental temperature of 82 K, which contributes to dI/dV by

$3.5 \cdot k_B T = 25$ meV and d^2I/dV^2 by $5.4 \cdot k_B T = 35$ meV¹⁶, prevents from a one-to-one assignment of the observed IETS peaks to the specific phonons in calculated DOS. A rough comparison between the DFT and IETS results implies that the IETS signals are mainly from optical phonons, but the exact assignment would require further investigation such as higher energy resolution IETS at a lower temperature, or the combination with Raman spectroscopy. Nevertheless, the current work shows that mechanic strain applied by an STM tip through a 2D semiconducting layer to the substrate is capable of both exciting phonons and detecting phonon modes at the nanoscale.

4. Conclusion

In summary, we employed monolayer MoS₂ as a tunneling barrier to conduct IETS with STM, which revealed the phonons in graphite substrate. STM tip height was controlled to apply local strain on graphite through the MoS₂ barrier, and such tip-induced strain resulted in a decrease in phonon energy and was detected in the peak shift of IETS. Calculated phonon DOS by DFT were compared with the IETS results, and both show phonon modes shifting to lower energy as the strain is increased. The qualitative agreement in the simulated and experimentally derived mechanic strains confirms that the IETS signal originates from the phonon excitations on the substrate. The results indicate that STM provides an efficient method to investigate the strain effect on both electronic and phononic properties when insulating/semiconducting 2D monolayers offer a tunneling barrier. Coupled with the high spatial resolution of STM, the IETS technique can expand our understanding of effects of local strain and provide spatially resolved information on the performance of nanodevices in the strained environment^{1,5}.

Acknowledgement: This research was conducted at the Center for Nanophase Materials Sciences, which is a DOE Office of Science User Facility. This research used resources of the National Energy Research Scientific Computing Center, a DOE Office of Science User Facility supported by the Office of Science of the U.S. DOE under Contract No. DE-AC02-05CH11231.

References

1. D. Akinwande, N. Petrone, and J. Hone, *Two-dimensional flexible nanoelectronics*. Nature Communications **5**, 5678 (2014).
2. F. Guinea, M. I. Katsnelson, and A. K. Geim, *Energy gaps and a zero-field quantum Hall effect in graphene by strain engineering*. Nature Physics **6**, 30 (2010).
3. H. Li, A. W. Contryman, X. Qian, S. M. Ardakani, Y. Gong, X. Wang, J. M. Weisse, C. H. Lee, J. Zhao, P. M. Ajayan, J. Li, H. C. Manoharan, and X. Zheng, *Optoelectronic crystal of artificial atoms in strain-textured molybdenum disulphide*. Nature Communications **6**, 7381 (2015).
4. N. Levy, S. A. Burke, K. L. Meaker, M. Panlasigui, A. Zettl, F. Guinea, A. H. C. Neto, and M. F. Crommie, *Strain-Induced Pseudo-Magnetic Fields Greater Than 300 Tesla in Graphene Nanobubbles*. Science **329**, 544 (2010).
5. R. Rafael, C.-G. Andrés, C. Emmanuele, and G. Francisco, *Strain engineering in semiconducting two-dimensional crystals*. Journal of Physics: Condensed Matter **27**, 313201 (2015).
6. A. Castellanos-Gomez, M. Poot, G. A. Steele, H. S. J. van der Zant, N. Agrait, and G. Rubio-Bollinger, *Mechanical properties of freely suspended semiconducting graphene-like layers based on MoS₂*. Nanoscale Research Letters **7**, 233 (2012).
7. C. Lee, X. Wei, J. W. Kysar, and J. Hone, *Measurement of the Elastic Properties and Intrinsic Strength of Monolayer Graphene*. Science **321**, 385 (2008).
8. S. Bertolazzi, J. Brivio, and A. Kis, *Stretching and Breaking of Ultrathin MoS₂*. ACS Nano **5**, 9703 (2011).
9. K. Elibol, B. C. Bayer, S. Hummel, J. Kotakoski, G. Argentero, and J. C. Meyer, *Visualising the strain distribution in suspended two-dimensional materials under local deformation*. Sci. Rep. **6** (2016).
10. U. Chandni, K. Watanabe, T. Taniguchi, and J. P. Eisenstein, *Signatures of Phonon and Defect-Assisted Tunneling in Planar Metal-Hexagonal Boron Nitride-Graphene Junctions*. Nano Letters **16**, 7982 (2016).
11. H. W. Kim, W. Ko, J. Ku, I. Jeon, D. Kim, H. Kwon, Y. Oh, S. Ryu, Y. Kuk, S. W. Hwang, and H. Suh, *Nanoscale control of phonon excitations in graphene*. Nature Communications **6**, 7528 (2015).
12. F. D. Natterer, Y. Zhao, J. Wyrick, Y.-H. Chan, W.-Y. Ruan, M.-Y. Chou, K. Watanabe, T. Taniguchi, N. B. Zhitenev, and J. A. Stroscio, *Strong Asymmetric Charge Carrier Dependence in Inelastic Electron Tunneling Spectroscopy of Graphene Phonons*. Physical Review Letters **114**, 245502 (2015).
13. L. Vitali, M. A. Schneider, K. Kern, L. Wirtz, and A. Rubio, *Phonon and plasmon excitation in inelastic electron tunneling spectroscopy of graphite*. Physical Review B **69**, 121414 (2004).
14. Y. Zhang, V. W. Brar, F. Wang, C. Girit, Y. Yayon, M. Panlasigui, A. Zettl, and M. F. Crommie, *Giant phonon-induced conductance in scanning tunnelling spectroscopy of gate-tunable graphene*. Nature Physics **4**, 627 (2008).
15. S. Jung, M. Park, J. Park, T.-Y. Jeong, H.-J. Kim, K. Watanabe, T. Taniguchi, D. H. Ha, C. Hwang, and Y.-S. Kim, *Vibrational Properties of h-BN and h-BN-Graphene Heterostructures Probed by Inelastic Electron Tunneling Spectroscopy*. Scientific Reports **5**, 16642 (2015).
16. B. C. Stipe, M. A. Rezaei, and W. Ho, *Single-Molecule Vibrational Spectroscopy and Microscopy*. Science **280**, 1732 (1998).
17. C.-I. Chiang, C. Xu, Z. Han, and W. Ho, *Real-space imaging of molecular structure and chemical bonding by single-molecule inelastic tunneling probe*. Science **344**, 885 (2014).

18. E. E. Vdovin, A. Mishchenko, M. T. Greenaway, M. J. Zhu, D. Ghazaryan, A. Misra, Y. Cao, S. V. Morozov, O. Makarovskiy, T. M. Fromhold, A. Patané, G. J. Slotman, M. I. Katsnelson, A. K. Geim, K. S. Novoselov, and L. Eaves, *Phonon-Assisted Resonant Tunneling of Electrons in Graphene-Boron Nitride Transistors*. Phys. Rev. Lett. **116**, 186603 (2016).
19. E. Del Corro, M. Taravillo, and V. G. Baonza, *Nonlinear strain effects in double-resonance Raman bands of graphite, graphene, and related materials*. Phys. Rev. B **85** (2012).
20. T. M. G. Mohiuddin, A. Lombardo, R. R. Nair, A. Bonetti, G. Savini, R. Jalil, N. Bonini, D. M. Basko, C. Galiotis, N. Marzari, K. S. Novoselov, A. K. Geim, and A. C. Ferrari, *Uniaxial strain in graphene by Raman spectroscopy: G peak splitting, Grüneisen parameters, and sample orientation*. Phys. Rev. B **79** (2009).
21. H. Sakata, G. Dresselhaus, M. S. Dresselhaus, and M. Endo, *Effect of uniaxial stress on the Raman spectra of graphite fibers*. J. Appl. Phys. **63**, 2769 (1988).
22. O. Frank, G. Tsoukleri, I. Riaz, K. Papagelis, J. Parthenios, A. C. Ferrari, A. K. Geim, K. S. Novoselov, and C. Galiotis, *Development of a universal stress sensor for graphene and carbon fibres*. Nat. Commun. **2** (2011).
23. X. Li, M.-W. Lin, L. Basile, S. M. Hus, A. A. Puretzky, J. Lee, Y.-C. Kuo, L.-Y. Chang, K. Wang, J. C. Idrobo, A.-P. Li, C.-H. Chen, C. M. Rouleau, D. B. Geohegan, and K. Xiao, *Isoelectronic Tungsten Doping in Monolayer MoSe₂ for Carrier Type Modulation*. Advanced Materials **28**, 8240 (2016).
24. H. Li, Y. Li, A. Aljarb, Y. Shi, and L.-J. Li, *Epitaxial Growth of Two-Dimensional Layered Transition-Metal Dichalcogenides: Growth Mechanism, Controllability, and Scalability*. Chem. Rev. **Article ASAP** (2017).
25. C. Zhang, A. Johnson, C.-L. Hsu, L.-J. Li, and C.-K. Shih, *Direct Imaging of Band Profile in Single Layer MoS₂ on Graphite: Quasiparticle Energy Gap, Metallic Edge States, and Edge Band Bending*. Nano Letters **14**, 2443 (2014).
26. C.-P. Lu, G. Li, J. Mao, L.-M. Wang, and E. Y. Andrei, *Bandgap, Mid-Gap States, and Gating Effects in MoS₂*. Nano Letters **14**, 4628 (2014).
27. X. Zhou, K. Kang, S. Xie, A. Dadgar, N. R. Monahan, X. Y. Zhu, J. Park, and A. N. Pasupathy, *Atomic-Scale Spectroscopy of Gated Monolayer MoS₂*. Nano Letters **16**, 3148 (2016).
28. Q. H. Wang, K. Kalantar-Zadeh, A. Kis, J. N. Coleman, and M. S. Strano, *Electronics and optoelectronics of two-dimensional transition metal dichalcogenides*. Nat. Nanotechnol. **7**, 699 (2012).
29. C. Zhang, Y. Chen, A. Johnson, M.-Y. Li, L.-J. Li, P. C. Mende, R. M. Feenstra, and C.-K. Shih, *Probing Critical Point Energies of Transition Metal Dichalcogenides: Surprising Indirect Gap of Single Layer WSe₂*. Nano Letters **15**, 6494 (2015).
30. X. Ling, Y.-H. Lee, Y. Lin, W. Fang, L. Yu, M. S. Dresselhaus, and J. Kong, *Role of the Seeding Promoter in MoS₂ Growth by Chemical Vapor Deposition*. Nano Letters **14**, 464 (2014).
31. T.-H. Kim, Z. Wang, J. F. Wendelken, H. H. Weitering, W. Li, and A.-P. Li, *A cryogenic Quadrupole scanning tunneling microscope system with fabrication capability for nanotransport research*. Rev. Sci. Instrum. **78**, 123701 (2007).
32. A.-P. Li, K. W. Clark, X. G. Zhang, and A. P. Baddorf, *Electron Transport at the Nanometer-Scale Spatially Revealed by Four-Probe Scanning Tunneling Microscopy*. Advanced Functional Materials **23**, 2509 (2013).
33. T.-H. Kim, M. Angst, B. Hu, R. Jin, X.-G. Zhang, J. F. Wendelken, E. W. Plummer, and A.-P. Li, *Imaging and manipulation of the competing electronic phases near the Mott metal-insulator transition*. Proceedings of the National Academy of Sciences **107**, 5272 (2010).
34. A. Togo and I. Tanaka, *First principles phonon calculations in materials science*. Scripta Materialia **108**, 1 (2015).
35. P. Trucano and R. Chen, *Structure of graphite by neutron diffraction*. Nature **258**, 136 (1975).
36. J. P. Perdew, K. Burke, and M. Ernzerhof, *Generalized Gradient Approximation Made Simple*. Physical Review Letters **77**, 3865 (1996).
37. P. E. Blöchl, *Projector augmented-wave method*. Physical Review B **50**, 17953 (1994).
38. G. Kresse and J. Furthmüller, *Efficient iterative schemes for ab initio total-energy calculations using a plane-wave basis set*. Physical Review B **54**, 11169 (1996).
39. G. Kresse and D. Joubert, *From ultrasoft pseudopotentials to the projector augmented-wave method*. Physical Review B **59**, 1758 (1999).
40. P. A. Young, *Lattice parameter measurements on molybdenum disulphide*. Journal of Physics D: Applied Physics **1**, 936 (1968).
41. J. Hong, Z. Hu, M. Probert, K. Li, D. Lv, X. Yang, L. Gu, N. Mao, Q. Feng, L. Xie, J. Zhang, D. Wu, Z. Zhang, C. Jin, W. Ji, X. Zhang, J. Yuan, and Z. Zhang, *Exploring atomic defects in molybdenum*

- disulphide monolayers*. Nat. Commun. **6**, 6293 (2015).
42. L. Wirtz and A. Rubio, *The phonon dispersion of graphite revisited*. Solid State Communications **131**, 141 (2004).
 43. Y. Cai, J. Lan, G. Zhang, and Y.-W. Zhang, *Lattice vibrational modes and phonon thermal conductivity of monolayer MoS₂*. Physical Review B **89**, 035438 (2014).
 44. A. Molina-Sánchez and L. Wirtz, *Phonons in single-layer and few-layer MoS₂ and WS₂*. Phys. Rev. B **84**, 155413 (2011).
 45. N. Wakabayashi, H. G. Smith, and R. M. Nicklow, *Lattice dynamics of hexagonal MoS₂ studied by neutron scattering*. Physical Review B **12**, 659 (1975).